UNIVERSITY OF WEST ATTICA
eISSN:3136-7658

Applied Manufacturing Intelligence Journal

Vol. 5, No. 1, January, 2026



DLinear KAN Model for Ore Crusher Liner Wear Estimation Based on Motor Power and Vibration History

Miloslav Sládek[a,*], Dušan Rychlý[a]

[a] *Faculty of Mechanical Engineering, Technical University of Liberec, Liberec, 461 17, Czech Republic*

Received 12 November 2025; Revised 10 February 2026; Accepted 15 February 2026; Published 18 February 2026

Abstract

Wear of the ore crusher liner alters the crushing-chamber profile and can change energy demand, vibration transmission, and product-size consistency. This study develops a DLinear-KAN estimator that uses 48 h histories of motor power, power variance, vibration root-mean-square value, envelope kurtosis, high-frequency band energy, and a load descriptor to estimate liner wear. The DLinear path retains slowly varying operating information, whereas the KAN path represents nonlinear residual interactions before the two embeddings are fused by a regression head. A constructed single-campaign evaluation contains 1,248 hourly records, six synchronized variables, and 14 inspection-style checkpoints spanning 2.1–24.7 mm of wear. Using a chronological 70/10/20 training, validation, and test partition, the proposed model achieved a mean absolute error of 1.42 mm, a root means square error of 1.86 mm, and an R^2 value of 0.946. At an illustrative 18 mm warning boundary, the threshold error was 4.1% of all test windows. These results support the use of fused electrical and vibration histories as advisory evidence for inspection planning; they do not establish a universal replacement threshold or cross-site deployment performance. The study therefore provides a transparent demonstration of trend-residual fusion under sparse inspection-style labels and identifies the need for validation across liners, crushers, and operating conditions.

Keywords: Crusher Liner Wear, Motor Power Signature, Vibration History, DLinear-KAN, Condition Monitoring

1. Introduction

Crusher liner wear modifies the chamber shape, which, in turn, alters the ore-breakage characteristics and energy-demand and product-size-distribution characteristics of the mineral-processing circuit [1]. Research on the wear of chamber profiles has shown that progressive material loss is related to changes in ore contact and nip conditions under different feed hardnesses [2]. Maintenance methods based on inspection intervals should consider the uneven wear of the liner surface and the effect of operating conditions on the useful service life [3]. Electrical and vibration monitoring can also collect process data; however, the interpretation of this information needs to consider changes in load and structure [4]. Motor power is already recorded in many crushing circuits, so historical electrical data can be used to estimate the current condition. Vibration data contain information on impulse contact and frequency-dependent excitation that average power does not. Neither of the above is a direct index of the linear profile; Power is affected by feed rate, moisture content, cavity filling and control parameters, and vibration can also be caused by loose connections, bearing problems, mounting stiffness and transient impacts. Therefore, multi-sensor condition estimation requires a form that can keep the different time-varying characteristics of electrical and mechanical signals [5]. An increase in power or vibration should not be assumed to have reached the replacement limit of the liner. The question is whether the

* Corresponding author: miloslav.sla@tul.cz

https://doi.org/10.68406/amij.2026.vol5iss1np5:54-67

➢ This is an open access article under the CC BY-NC-SA 4.0 license (https://creativecommons.org/licenses/by/4.0/).

© Authors retain all copyrights.

continuous changes in the monitored history can be considered reliable evidence of geometric degradation under the given operating conditions.

Data-driven wear estimation has become more attractive with the provision of extended operating history and stable timestamps by plant historians, edge recorders and supervisory control systems. Crusher data are not suitable for the general-purpose prediction model because the target variable changes slowly and the explanatory variables change rapidly. A liner will lose approximately 1-2 mm of profile per week, and after feeding segregation or cavity filling for a few seconds, there will be an alteration in motor current and vibration envelope. A model that gives too much weight to the short-term data will be very reactive and unstable. If it is too smooth, then some vibration characteristics that occur only when the chamber is near failure will be missed. Previously, regression and neural network methods generally used hand-crafted features obtained from selected operating windows [6]. Recently, temporal models have been able to use historical information directly, but they often treat the whole sequence as a single type of information source [7]. The above assumption is not applicable to a crusher; although the trend of motor power with respect to chamber load can be determined relatively easily, the vibration history contains complex frequency-localized information [8]. A model that can distinguish between the contributions is more appropriate than a single recurrent or attention-based architecture [9]. Therefore, in this paper, we consider the estimation of liner wear to be a type of hybrid trend-nonlinearity problem rather than a general time-series regression problem [10].

This paper proposes a DLinear-KAN model for estimating ore crusher liner wear from motor-power and vibration histories. Its central design choice is to separate slowly varying operational information from localized nonlinear deviations before prediction. The DLinear branch processes the decomposed trend, whereas the KAN branch transforms residual interactions among vibration features, short power fluctuations, and load descriptors. This differs from a stand-alone linear sequence model or an undifferentiated nonlinear fusion model, both of which may mix gradual campaign progression with transient operating effects. The proposed structure treats motor power and vibration as indirect evidence of degradation rather than direct geometric measurements, and it therefore retains operating context in the historical input.

The following sections introduce the estimation problem in the context of monitoring, prepare historical signals and build a model, and examine the predictive error and maintenance significance. Section 2 presents engineering methods for crusher condition monitoring and learning-based wear estimation to address the problem of a slow degradation rate and fluctuating operational signals. Section 3 introduces the problem of liner wear estimation, defines the representation of historical signals, and explains how motor power and vibration records are prepared for model input. Section 4 introduces the DLinear-KAN architecture and the decomposition, nonlinear fusion, loss construction and deployment logic. Section 5 shows the experimental data, comparison results, ablation analysis, error distribution, threshold behavior and sensitivity observation. Section 6 presents the summary of the study, shortcomings and future work.

2. Related Work

2.1. Crusher condition monitoring with power and vibration

Traditionally, condition monitoring of crushing equipment has consisted of electrical measurements, vibration analysis, lubrication observation and periodic mechanical tests. Motors have the advantages of a low cost and high durability, and can achieve good crushing resistance for a given feed condition. Research on comminution energy has often used power consumption as an indicator of chamber load, changes in product size, and control stability [11]. At the same power, different wear conditions can occur due to changes in feed rate, ore competence and closed-side setting of liner wear estimation. Therefore, the power-only indicators need to be normalized by area, and the fixed alarm threshold will be different after a campaign modification.

Vibration monitoring also provides a type of data by detecting impacts, contact changes, responses of rotating machinery and structural transmission paths. Envelope statistics, spectral bands, crest factor, kurtosis and time-frequency energy have been used to identify abnormal mechanical conditions in heavy-duty rotating equipment [12]. Vibration in the crusher liner can also be employed to detect wear of the chamber surface, alteration in impact regularity, and frame excitation under a normal operating power. Power is less specific than vibration, and the defect characteristics of bearing damage, loose fasteners, mounting changes and ore bridging may be similar. Therefore, the model should be able to learn from the context of the vibration history and avoid attributing a single high-energy sample to wear.

Some monitoring systems combine power and vibration data using feature concatenation, principal component analysis or rule-based voting. The above methods are feasible but often assume that the relationship between features and wear is stationary throughout the campaign [13]. In real plants, the first third of the liner life may show a weak signal drift, the middle stage may be stable abrasion, and in the final stage, sharper nonlinear changes occur because the chamber geometry has moved away from the nominal crushing profile. This stage-dependent behavior leads to the use of temporal models with a longer history to consider both monotonic degradation and non-linear local responses.

2.2. Learning models for industrial wear estimation

With the rise of industrial data, learning-based wear estimation has developed from shallow regression to temporal deep models. Support Vector Regression, Random Forests and Gradient Boosting are still applicable in cases of limited labels and well-engineered features [14]. The problem is that the history windows need to be reduced to statistics before training, and thus the order effect of continuous overstimulation or multiple short impacts is no longer shown. Recurrent networks are suitable for directly handling sequences and have been applied to the study of equipment degradation problems; however, it is difficult to interpret their hidden states directly, and they may be unstable under irregular sampling intervals or when the target changes very slowly compared to the input.

Temporal Convolutional Networks and Transformer variants improve parallel training and can model long-range dependencies [15]. A large volume of data and careful regularization are needed for the crusher application due to relatively sparse inspection labels. Many mines have years of power and vibration data, but only a few reliable liner profiles due to the labor-intensive shutdown inspection. Shao et al. [16] benchmarked heterogeneous multivariate time-series forecasting settings, highlighting the need to distinguish different temporal components in industrial data. Wear and tear are also a problem; a large number of the targets show a slow, gradual increase rather than a sudden rise.

Kolmogorov-Arnold networks are also suitable, and the fixed activation and matrix-weight behaviors at the edges can be replaced by learnable univariate functions [17]. To address the non-linear relationship between vibration bands and wear in industrial signals without resorting to a black-box dense layer, such functions can be employed. The other problem is that decomposition models and KAN structures have rarely been combined to estimate crusher liner wear from motor power and vibration history. The DLinear-KAN model introduced above separates the problems of slow-trend extraction and nonlinear residual interpretation into different modules in the architecture.

3. Problem Formulation and Historical Signal Preparation

3.1. Wear target and sensing window

The estimation task is defined for an ore crusher observed through an ordered sequence of production states. At each hourly index, the monitoring system acquires six synchronized variables: motor power, power variance, vibration root-mean-square value, envelope kurtosis, high-frequency band energy, and a load descriptor. The target is an inspection-derived equivalent liner-depth loss rather than a continuously observed three-dimensional profile. A 48 h rolling history is used to form each model input so that progressive changes and short-lived signal excursions can be interpreted together. This construction does not make any individual variable a direct wear measurement; it provides an ordered multi-sensor context from which one continuous wear estimate is inferred.

According to the engineering practice of expressing the liner condition as an equivalent depth loss, a full three-dimensional profile is not required to achieve the purpose of definition. A full profile is very detailed, but it is not available often enough for the model to be trained. An equivalent depth target can reduce the number of measured profile points to one for comparison of inspections and use by maintenance engineers. Do not use this value for all local grooves and edge-rounding patterns. To determine if the distance from the chamber to the original position is too large for observation, and if so, to develop a replacement plan. Therefore, the estimator is relatively stable in the presence of small load fluctuations and is very sensitive near the warning area; however, it does not achieve a low overall error for the entire campaign.

Let x_t denote the synchronized condition vector at time t, and let y_t denote the corresponding liner wear estimate. The rolling input matrix X_t contains the most recent L observations, with rows ordered from the oldest to the newest record. The following equation states the historical input-output mapping used throughout the estimator.

$$X_t = [x_{t-L+1}, x_{t-L+2}, \dots, x_t], \hat{y}_t = f_\theta(X_t) \quad (1)$$

In this equation, the chronological ordering of the window is explicit: x_{t-L+1} is the oldest record and x_t is the newest. The learned mapping f_θ returns one continuous wear estimate from the complete multivariate history rather than from a single synchronous sample.

3.2. Power and vibration normalization

Raw power and vibration records are not used directly because operating level changes can dominate degradation information. Power is treated as a load-dependent signal, whereas vibration features are retained as indicators of impulsive and frequency-localized behavior. Robust normalization is fitted using the training portion and then applied unchanged to validation and test windows, thereby limiting the influence of rare excursions and reducing the possibility that site-specific control settings are learned as apparent wear. The transformation is an input-conditioning step, not a physical correction of the crusher process; feed changes, mounting effects, and sensor drift can still affect the normalized features and must be interpreted alongside the recorded operating context.

$$z_{t,k} = \frac{x_{t,k} - median(x_k)}{IQR(x_k) + \varepsilon} \quad (2)$$

The normalization equation above fixes the transformation before validation and testing. Its median-centered form reduces the influence of rare power or vibration excursions, while the positive ε term prevents an unstable scale when a feature has limited spread.

Normalization can also help to reduce the problem of site-specific operating policies being learned by the model rather than wear mechanisms. For instance, near the end of a liner changeover, because operators have already suspected a problem with the chamber, the crusher is run at a reduced feed rate. Without context, if only the raw feed rate and raw power are used, the model may incorrectly assume a lower production rate due to reduced wear. In the preparation stage, the condition information is separated from the load information by using an explicit input for the load descriptor and normalizing the power and vibration variables in the training campaign. The same transformation parameters are then used for validation and testing. In this way, the order of events will be clear; otherwise, the later-stage conditions used for testing may affect the scale established in training.

3.3. Decomposition of slow and fast components

The preparation stage also separates slow and fast components before model fusion. A moving-average operator extracts the low-frequency trend associated with gradual chamber changes and persistent load shift. The residual keeps short-duration deviations that may contain impact and vibration evidence. This separation is important because the physical process of liner wear is gradual, while the recorded signals may contain bursts caused by feed interruption or short overload. The decomposition does not decide which component is more important; it gives the model two structured views of the same history.

$$X_t^{trend} = MA_w(X_t), X_t^{res} = X_t - X_t^{trend} \quad (3)$$

This decomposition equation produces two aligned histories from the same window. MA_w denotes the moving-average operation with width w; the residual term retains the difference between the observed signal and its local trend.

The window width used for the moving average is selected to be shorter than the model history but long enough to suppress isolated spikes. In the implementation, the operator is applied independently to each feature channel to avoid mixing power and vibration before the model has learned their respective roles. The trend component is therefore a low-pass representation of each original signal, while the residual component preserves departures from that local baseline. This design is particularly useful for vibration variables because an isolated high-kurtosis event may be caused by ore bridging, but a repeated pattern of elevated kurtosis during a rising power trend can be meaningful evidence of liner wear. Decomposition creates the conditions for the later fusion branch to evaluate this distinction.

Figure 1 is used to describe the signal construction workflow from factory history records to the model preparation window. It includes the inspection profile, hourly motor power, vibration features, robust normalization, trend-residual decomposition, and the final rolling tensor supplied to the estimator.

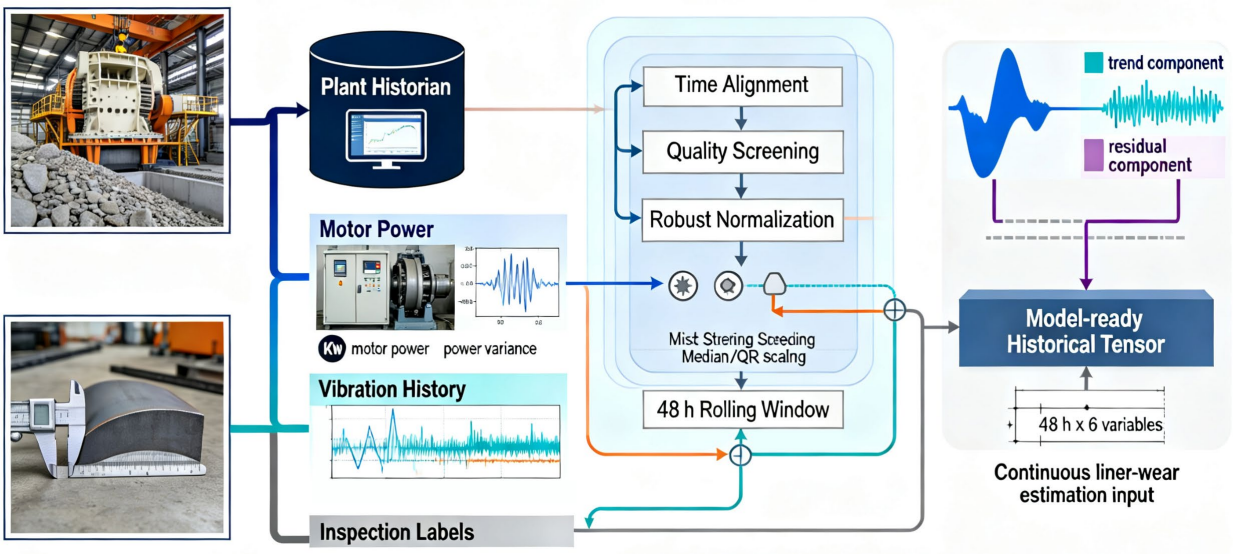


Figure 1. Signal preparation workflow for liner wear estimation from motor power and vibration history

4. DLinear KAN Estimation Model

4.1. DLinear trend branch

The DLinear branch is designed to learn the part of liner wear that is most closely associated with slow drift in motor power and operating condition. After decomposition, the trend matrix is passed through a linear temporal projection for each feature group. This design deliberately avoids an excessively deep representation for the trend component because a slow mechanical degradation target should not require a large number of nonlinear transformations to be represented. The branch output is a compact trend embedding that preserves the direction and magnitude of long-term change.

For feature group g, the trend embedding h_g is obtained through a linear mapping over the historical axis. The equation below maps each group before the outputs are concatenated and projected into the shared latent space used by the final estimator.

$$h_g = W_g X_{t,g}^{trend} + b_g, h_T = concat(h_1, h_2, \dots, h_G) \tag{4}$$

Within the trend equation, W_g and b_g are learned temporal projection parameters, while h_T preserves the ordered collection of group-level trend embeddings for the fusion stage.

The trend branch is also beneficial from an engineering audit perspective. A maintenance engineer can compare the branch behavior with known campaign progression, such as the gradual increase in power draw or the weakening of chamber stability near the end of service life. Although the learned weights are not a complete physical model, their linear structure makes it easier to detect whether the estimator has become dominated by a narrow time region or by a single feature. During model checking, large and inconsistent trend weights are treated as a sign that the history length, normalization, or label interpolation should be reviewed before deployment.

4.2. KAN residual and fusion branch

The residual branch handles nonlinear interactions among vibration history, short power fluctuations, and load descriptors after the slow trend has been separated. Instead of using only a multilayer perceptron, the proposed KAN component represents feature transformations through learnable spline-based univariate functions and then aggregates their responses for fusion. This branch is intended to retain localized signal structure that may be obscured by a purely trend-oriented representation. The resulting residual embedding should not be interpreted as a direct physical signature of liner geometry; it is a learned operational feature whose usefulness is evaluated through the controlled ablation comparison in the constructed dataset.

First, the residual input is flattened by feature group, and then spline-based transformation is performed with a fixed number of knots in the proposed arrangement. The KAN equation shows the nested edge functions in this branch. A small number of knots is used to represent the threshold effect of the KAN branch without needing to learn multiple operating windows. Therefore, the crusher data generally do not have repeated transient phenomena caused by liner geometry. A very flexible residual branch can solve the above problems and reduce generalization. Regularization of the spline functions is achieved by weight decay and validation monitoring, and the final branch dimension is kept smaller than the raw window dimension. The aim is to obtain the long-term non-linear residual pattern, not all short-term fluctuations.

$$h_N = \sum_{q=1}^{Q} \Phi_q \left(\sum_{p=1}^{P} \phi_{q,p}\left(X_{t,p}^{res}\right) \right) \tag{5}$$

Here the outer summation in the equation aggregates the transformed residual responses, whereas the inner summation combines the feature-specific spline functions. This arrangement assigns nonlinear interpretation to deviations that remain after trend extraction.

4.3. Loss function and deployment output

The final estimator fuses the DLinear trend embedding and the KAN residual embedding through a small regression head to produce one continuous wear estimate. The training objective combines absolute and squared error terms with an additional warning-region term so that errors near the advisory boundary receive explicit attention. The relative weighting of these terms is selected using the validation partition rather than the test partition. The loss supports a continuous regression task and does not convert the model into an automatic replacement controller; threshold-related output is retained as an inspection-support signal whose practical setting must be defined by the operating site.

$$\mathcal{L} = \alpha|y_t - \hat{y}_t| + (1-\alpha)(y_t - \hat{y}_t)^2 + \lambda I(|y_t - \tau| < \delta)|c_t - \hat{c}_t| \tag{6}$$

In the objective equation, α controls the balance between absolute and squared error, and λ weights the additional warning-region term. The indicator I activates that term only when the inspected wear y_t lies within δ of the selected threshold τ.

Deployment output is the Design of an advisory signal, not a binary instruction. Time-stamped wear prediction data contain operating conditions and the distance to the maintenance limit at a particular time. The output can be shown in the interface of the plant historian as a slow-moving condition trace with confidence bands based on validation residuals. Adjust or modify the model according to changes in the liner design, sensor relocation, significant control-policy alterations, or alterations in ore-source. The above conditions will not change the structure; only the statistics of power, vibration and wear will be altered. Therefore, the model puts forward a monitoring workflow to reduce inspection time by means of automatic estimation and retains human maintenance judgment for the final replacement decision.

Figure 2 shows the complete DLinear-KAN architecture. The flowchart separates trend extraction, residual interpretation, KAN nonlinear mapping, embedding fusion, wear-depth regression, and warning-threshold output, which makes the deployment path transparent for an engineering monitoring system.

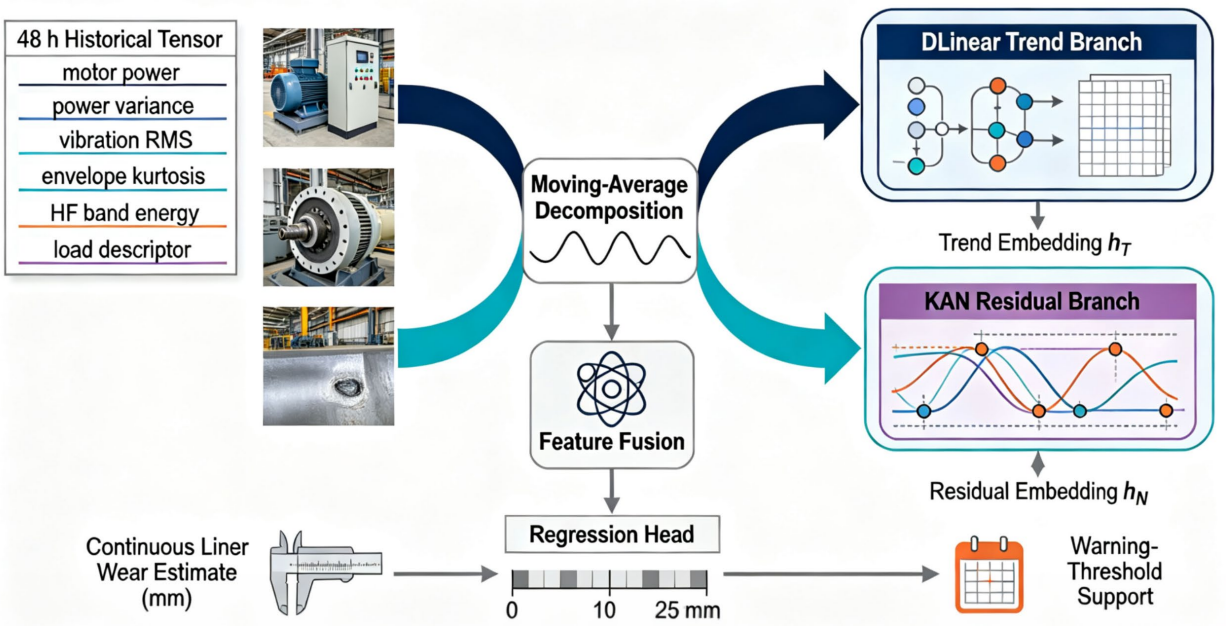


Figure 2. DLinear-KAN architecture for continuous liner wear estimation and warning-threshold support

5. Experimental Data and Analysis

5.1. Dataset and historical signal characterization

The constructed single-campaign demonstration contains 1,248 hourly records, six synchronous condition variables, and 14 inspection-type wear checkpoints ranging from 2.1 mm to 24.7 mm. Chronological evaluation is used to preserve the direction of information flow in degradation modelling [18]. The first 70% of records are used for training, the next 10% for validation, and the final 20% for testing, with a 48 h input history. Window construction and any label interpolation are restricted to the assigned chronological partition so that future inspection information cannot enter earlier model development. After excluding missing channels and physically invalid measurements, 1,176 usable windows remain. The sparse inspection-style checkpoints introduce uncertainty between observations, which is a known limitation of sparse degradation labels [19]; consequently, the window-level targets support a controlled demonstration rather than a fully observed continuous ground truth.

Table 1 separates campaign-level averages from the segment trajectories used in the plots. Motor power changes from 421.6 kW in the early region to 456.8 kW in the final region, an increase of 35.2 kW, while vibration RMS changes from 3.7 to 5.9 mm/s. Their relative changes differ substantially, so a common scaling factor would suppress useful mechanical variation. Figure 3(a) follows eight campaign segments: wear rises from 2.1 to 24.7 mm and normalized power trend rises from 0.05 to 0.52, a difference of 0.47 units. The increasing trajectory makes power history informative, but the graph does not establish that power uniquely identifies wear. Figure 3(b) separates RMS amplitude from high-frequency band energy using distinct ordinate scales; RMS rises from 3.5 to 6.2 mm/s and energy from 0.38 to 0.99. The later segments show larger changes in both indicators, providing a reason to retain band energy as well as amplitude. Segment endpoints and regional averages describe different aggregations and should not be treated as interchangeable observations.

Table 1. Monitoring variables and campaign-level descriptive statistics

Variable	Unit	Early region	Middle region	Final region
Motor power	kW	421.6	438.9	456.8
Power variance	kW^2	28.4	35.7	47.5
Vibration RMS	mm/s	3.7	4.6	5.9
Envelope kurtosis	-	3.1	3.7	4.4
HF band energy	g^2/Hz	0.42	0.58	0.91
Liner wear label	mm	5.3	13.8	22.1

Figure 3(c) compares envelope-kurtosis distributions with marked medians of 3.1 and 4.4. The shift in the central distribution indicates persistent changes in impulsiveness, whereas overlap between the distributions prevents a single kurtosis cutoff from identifying every high-wear window. The longer upper tail is particularly relevant because a few severe impacts can raise a summary statistic without representing a sustained chamber change. Distribution-based vibration monitoring evaluates both central tendency and tail behavior when impulsive events are intermittent [20]. Figure 3(d) places normalized power variance against high-frequency energy and colors each point by wear depth. Higher-wear points occupy the upper-right region more often, but the overlap at intermediate coordinates shows that two instantaneous descriptors cannot fully resolve the condition state. The scatter also explains why historical ordering matters: several successive windows in a rising region provide different evidence from one transient point. The model receives those ordered histories rather than only the coordinates of a current sample.

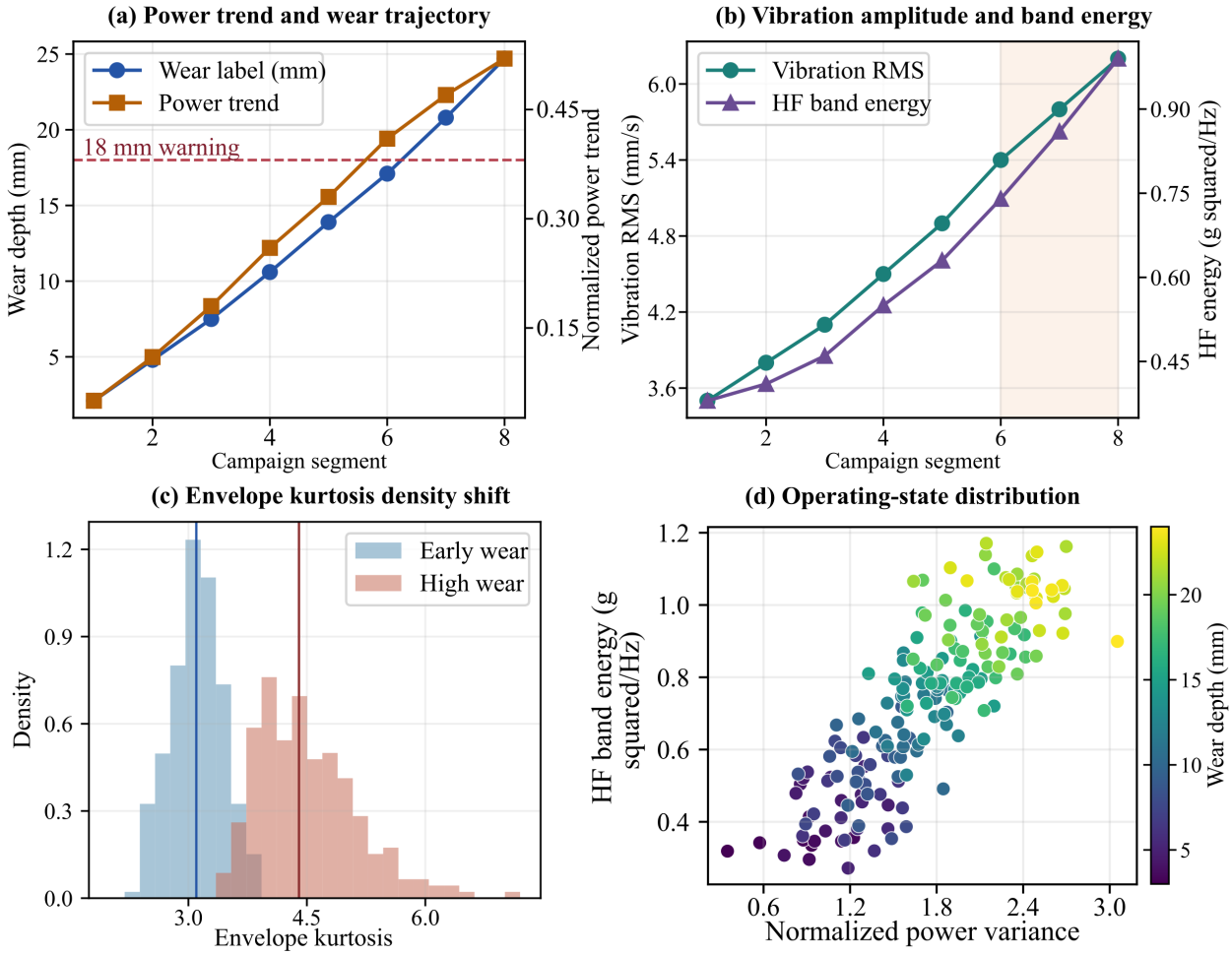


Figure 3. Dataset characterization: (a) power trend and wear trajectory; (b) vibration amplitude and band energy by wear stage; (c) envelope kurtosis density shift; (d) operating-state distribution under power variance and high-frequency energy

The preparation protocol will limit the range of the above comparisons. The average regional power is still based on the assumption of load normalization, and changes in control practice may affect the observed correlation with wear. Vibration is a kind of mechanical phenomenon, and due to varying impact times and transmission paths, it occurs more frequently. For this working example, the same six channels and history windows are provided to all the temporal

estimators, and feature-based regression only uses the statistics calculated from these windows. Validation selects a pre-processing method and model parameters, then tests on the test set. Changing the missing-data handling method will alter the available windows and the proportion of high-load periods; therefore, the retained-window count should be reported along with the error. The 14 checkpoint labels offer little additional wear data compared to the number of hourly windows. Close-packed windows use the same input records and interpolated target structures to reduce the evidential weight of minor differences in methods. To determine whether the obtained ranking is stable after modifications to the ore type, inspection period and operating policies, replicate experiments will be conducted with independent observations.

5.2. Comparative performance and component analysis

All seven estimators were compared under the same chronological partition, monitoring variables, and 48 h history length. Table 2 reports a mean absolute error of 1.42 mm for DLinear-KAN, compared with 2.48 mm for support vector regression, 2.05 mm for the recurrent network, 1.91 mm for temporal convolution, 1.77 mm for the Transformer encoder, 1.83 mm for pure DLinear, and 1.61 mm for MLP fusion. The proposed model also has a root mean square error of 1.86 mm and a coefficient of determination of 0.946. Controlled ablation is useful for isolating an architectural component while preprocessing and evaluation conditions are held constant [21]. These are descriptive outcomes from one constructed chronological split; parameter counts and tuning budgets were not matched, and the results do not establish statistical superiority. The ablation comparison nevertheless indicates that removing vibration history or replacing the KAN residual mapping increases error within the same evaluation protocol.

Table 2. Test-set performance of liner wear estimation models

Model	MAE *mm*	RMSE *mm*	R^2	Threshold error *%*
SVR with engineered features	2.48	3.12	0.842	13.6
LSTM	2.05	2.61	0.889	10.9
Temporal convolutional network	1.91	2.43	0.904	9.8
Transformer encoder	1.77	2.30	0.917	8.6
Pure DLinear	1.83	2.35	0.912	9.1
MLP fusion variant	1.61	2.08	0.932	6.8
DLinear-KAN	1.42	1.86	0.946	4.1

Figure 4(a) compares inspected-style labels with predicted wear across 110 illustrative windows, including a one-to-one reference and a shaded +/-2 mm tolerance corridor. Points between 19 and 22 mm warrant particular attention because deviations in that interval can alter whether an inspection warning is issued. Scatter around the diagonal provides a visual check for systematic underestimation that a global coefficient of determination can conceal. Figure 4(b) displays the error distribution for all seven methods, with the proposed model having an interquartile interval of -0.73 to 0.81 mm and the temporal convolutional model an interval of -1.21 to 1.36 mm. The narrower central interval concerns routine error, while the whiskers describe more extreme deviations; neither substitute for a threshold-specific count. Separating dispersion from bias is customary in agreement analysis because a distribution centered near zero may still contain errors too large for a given decision boundary [22]. The plot therefore includes the zero-error reference and both tolerance limits rather than presenting only model medians.

Figure 4(c) partitions decisions at the 18 mm boundary into 52.4% true alerts, 2.2% false alerts, 1.9% missed alerts, and 43.5% correct normal decisions. The erroneous shares sum to 4.1%, matching the threshold error in Table 2. These percentages use all test windows as the denominator; the missed-alert share is not the conditional false-negative rate among truly worn cases. On that conditional denominator, 1.9 divided by the combined true-alert and missed-alert share corresponds to approximately 3.5%. Making the denominator explicit matters when the class prevalence changes between campaigns. Threshold evaluation in maintenance models distinguishes missed detections from unnecessary interventions because their operational consequences differ [23]. False alerts can consume inspection time, whereas missed alerts allow an uncertain wear state to persist. The confusion profile supports that distinction without assuming equal costs or assigning an unsupported replacement policy to the illustrative dataset.

Figure 4(d) is the full model without any components removed. Excluding vibration history, the mean absolute error is 1.68mm instead of 1.42mm; replacing KAN with an MLP raises it to 1.61mm; and without decomposition, it increases to 1.89mm. The corresponding increases are 18.3%, 13.4% and 33.1%. Decomposition has the largest observed effect; it is difficult to learn gradual progression and intermittent changes from the same undifferentiated history. No physical wear mechanism is presented in the association, and spline transformations are not inherently more interpretable. The KAN replacement test uses a particular implementation and tuning configuration, and the vibration removal changes the

information available to the estimator. In a plant deployment, if a sensor branch is removed, new threshold calibration and an error assessment need to be carried out. The tolerance corridor in the scatter plot and the decision categories in the warning plot have different effects of this modification; although the estimates are still close in absolute depth, they fall on opposite sides of the maintenance boundary.

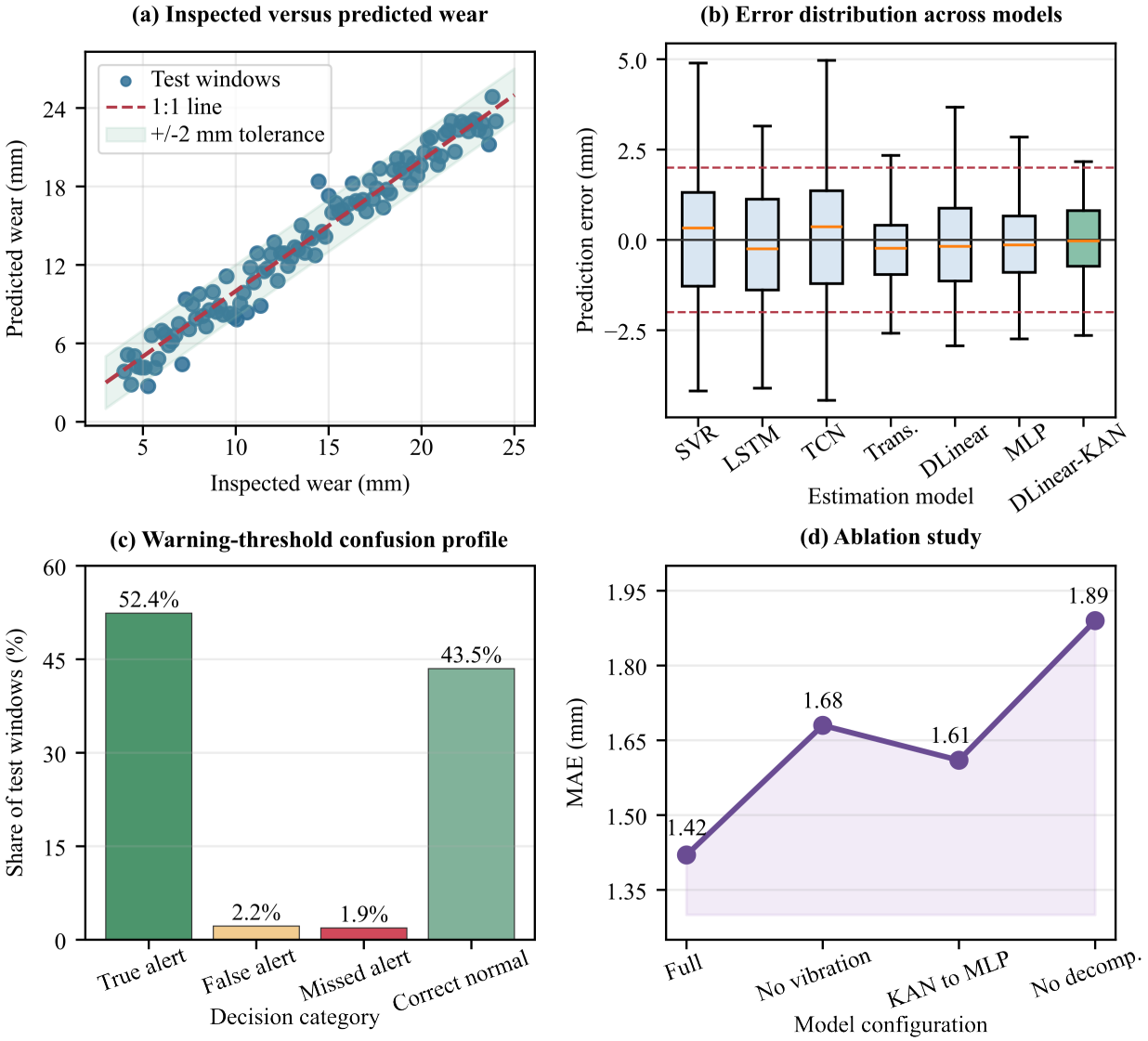


Figure 4. Model comparison and ablation results: (a) inspected versus predicted wear; (b) error distribution across baseline models; (c) replacement-warning threshold confusion profile; (d) ablation study of model components

5.3. Residual sensitivity and robustness under load changes

Residual diagnostics examine where error increases within the evaluated history rather than treating the average as uniform across operation. Figure 5(a) shows the ordered residuals with a shaded +/-2 mm tolerance band and two marked disturbance intervals. Exceedances cluster around those intervals, which suggests sensitivity to abrupt operating changes but does not establish ore hardness as their cause without an independent hardness record. Agreement analysis uses the mean difference and limits of agreement to assess systematic bias and the spread of individual discrepancies [24]. Figure 5(b) marks a bias of -0.08 mm and limits of -3.45 and 3.29 mm in the illustrative agreement display. The near-zero bias coexists with a much wider individual-error envelope; an estimate close to a warning boundary can therefore be uncertain even when the overall mean is well centered. Figure 5(c) separates five wear-stage bins, with mean absolute errors of 1.21, 1.30, 1.38, 1.49, and 1.58 mm. The progression exposes deterioration in late-stage precision that is hidden in the single value reported for the full test region.

History length and channel removal examine two different sources of that sensitivity. Temporal context selection in degradation estimation balances the information provided by persistent trends against the influence of obsolete operating states [25]. Figure 5(d) compares histories of 12, 24, 48, 72, and 96 h, yielding mean absolute errors of 1.93, 1.61, 1.42, 1.44, and 1.46 mm. The improvement from 24 to 48 h is 0.19 mm, while extending the history beyond 48 h produces no comparable gain in this example. Figure 5(e) reports 1.42 mm for the full input, 1.61 mm without high-frequency energy,

1.56 mm without kurtosis, 1.52 mm without RMS, and 1.83 mm for power only. Removing band energy has the largest effect among the individual vibration removals, although its effect cannot be interpreted independently of correlations with the remaining channels. Figure 5(f) presents the contribution matrix for four stage-load partitions. Power-trend contribution declines from 0.42 in early low-load operation to 0.24 in late high-load operation, while RMS rises from 0.18 to 0.38 and band energy from 0.12 to 0.34. These attribution scores are displayed as separate sensitivity indicators, not normalized shares summing to unity or causal effects.

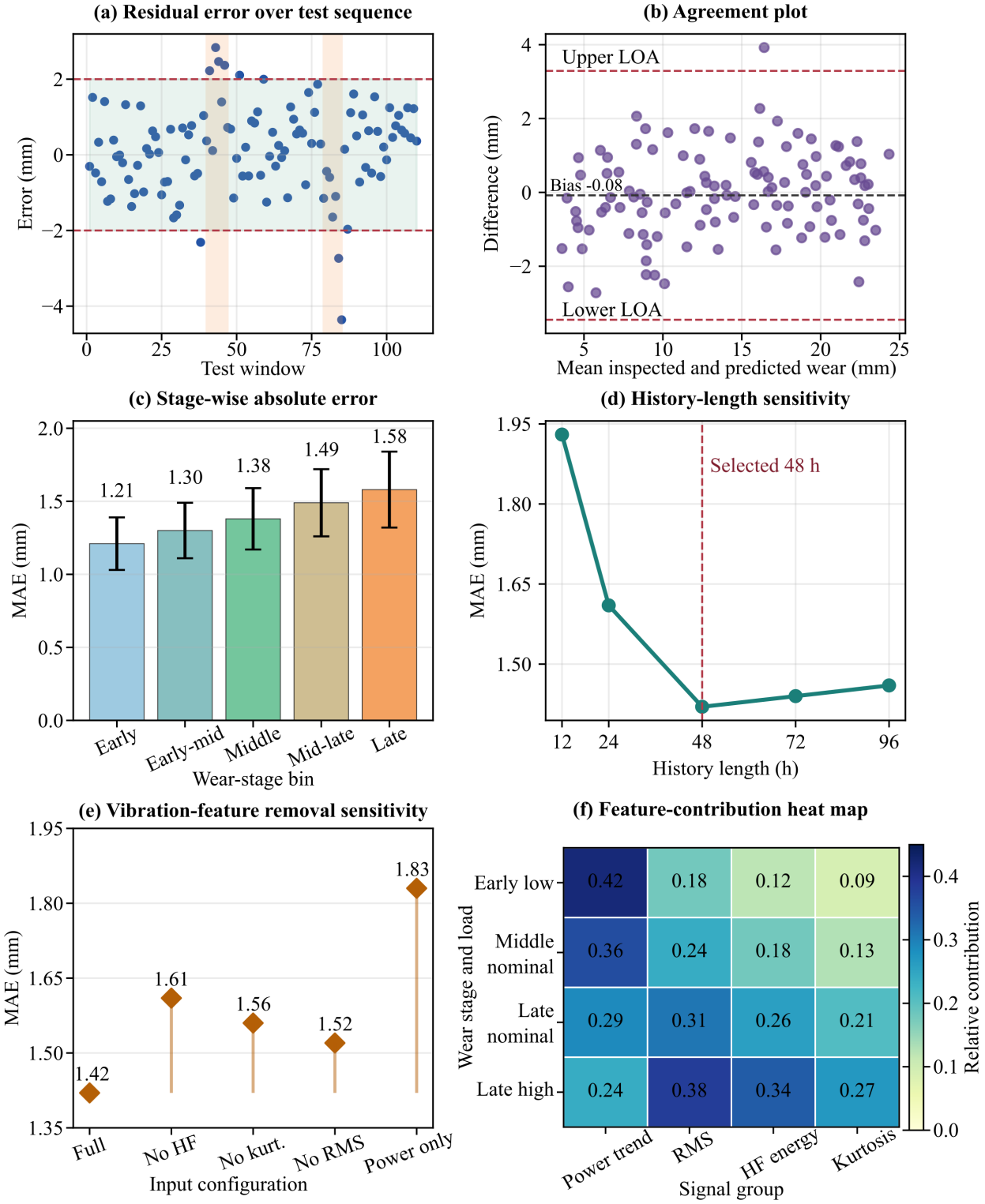


Figure 5. Error behavior and sensitivity: (a) residual error over test sequence; (b) agreement plot with bias and limits; (c) stage-wise absolute error; (d) history-length sensitivity; (e) vibration-feature removal sensitivity; (f) feature-contribution heat map by wear stage and load state

Load-stratified validation is used in machinery monitoring to expose conditional error that a pooled test metric can conceal [26]. Figure 6 compares error distributions under low, nominal, and high load, with medians of 1.03, 0.91, and

1.28 mm and 90th percentiles of 2.31, 2.18, and 2.84 mm. The larger center and upper region under high load indicate that operating state should accompany each estimate. Warning checks at wear depths of 16, 18, and 20 mm give balanced accuracies of 94.6%, 95.9%, and 93.8%, respectively. These values are illustrative classification results for the constructed dataset, not universal liner-replacement limits; any operational threshold must be set using site-specific geometry, maintenance risk, and inspection policy.

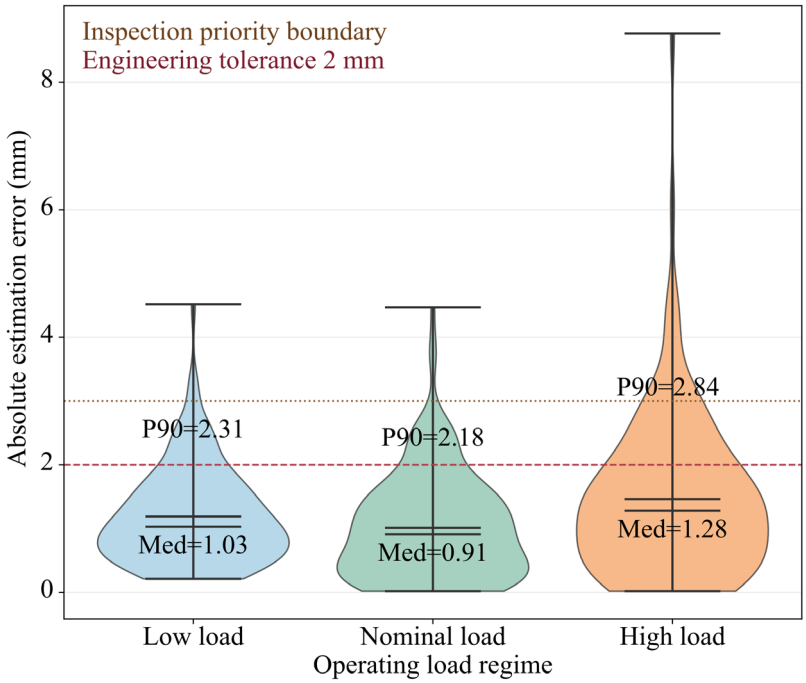


Figure 6. Engineering robustness across load regimes

Deployment uncertainty also includes load partition, sensor drift, mounting changes, missing-channel status, and changes in acquisition or aggregation. Sensor drift and acquisition changes can alter condition-monitoring features without changing the actual component state [27]. For each hourly estimate, the recorded history identifier, normalization version, missing-channel status, and load state should be retained so that an abnormal output can be traced to its data context. No stand-alone inference-time benchmark or edge-computing latency reduction was experimentally validated in this case. Near an advisory threshold, the operator display should present the predicted wear, its distance from the site-defined limit, the recent trend, and the available sensor-health context; a single high vibration channel should prompt verification rather than an immediate wear conclusion.

6. Conclusion

This study developed and evaluated a DLinear-KAN estimator that combines motor-power history and vibration history to infer ore crusher liner wear as a continuous monitoring variable.

1. The constructed chronological evaluation yielded a mean absolute error of 1.42 mm, a root means square error of 1.86 mm, and an R2 value of 0.946 for DLinear-KAN. At the 18 mm warning boundary, threshold classification error was 4.1%, indicating that the model retained a close correspondence with the inspection-calibrated wear trajectory while providing a maintenance-relevant output.

2. The comparative and ablation results showed that separating slow trend information from nonlinear residual information was consequential: pure DLinear reached 1.83 mm MAE, removal of vibration history increased MAE to 1.68 mm, and removal of trend-residual decomposition increased MAE to 1.89 mm. The 48-h history window gave the lowest tested error, whereas longer windows produced no further improvement, suggesting that useful monitoring context is finite and must be matched to the temporal behavior of the crusher signals.

3. The findings are limited to a constructed single-campaign evaluation with inspection-style labels, six monitored variables, and hourly aggregation. They do not demonstrate cross-site transfer, universal replacement thresholds, automatic shutdown capability, or measured inference-latency benefits. Sparse inspection checkpoints also limit confidence in target values between observations. Future work should evaluate the method across crusher types, liner materials, feed conditions, and independently measured liner profiles, while testing data-quality monitoring and calibration procedures before using the output for routine inspection planning.

The work provides a structured basis for integrating power and vibration evidence into inspection planning, while future studies should validate the method across crusher types, liner alloys, ore classes, and independently measured wear profiles.

7. Declarations

7.1 Author Contributions

Miloslav Sládek contributes to conceptualization, methodology, software, validation, analysis, investigation, data collection, draft preparation, manuscript editing, visualization, supervision, project administration, and funding acquisition. Dušan Rychlý contributes to validation, analysis, investigation, data collection, draft preparation. All authors have read and agreed with the manuscript before its submission and publication.

7.2 Funding and Acknowledgments

This research received no specific financial support from any funding agency.

7.3 Institutional Review Board Statement

Not applicable.

7.4 Informed Consent Statement

Not applicable.

7.5 Date Availability

Not applicable.

7.6 Declaration of Competing Interest

The authors declare that they have no known competing financial interests or personal relationships that could have appeared to influence the work reported in this paper.

7.7 Declaration of generative AI and AI-assisted technologies

During the preparation of this manuscript, the authors utilized Grammarly for linguistic polishing, logical organization and draft revision. The generative AI tool was not involved in research design, data collection, data analysis, or the equation of core conclusions. All outputs generated by AI were reviewed, revised and verified manually by the authors. The authors take full responsibility for all content of this manuscript.

8. References

[1] Denkena, B., Klemme, H., & Stoppel, D. (2025). Condition monitoring of grinding wheels: Potential of internal control signals. Production Engineering, 19(1), 65-75. https://doi.org/10.1007/s11740-024-01295-x

[2] Denkena, B., Wichmann, M., Rokicki, M., & Stürenburg, L. (2025). Modelling the influence of tool wear on shape errors in milling using a hybrid soft-sensor. Production Engineering, 19(1), 101-110. https://doi.org/10.1007/s11740-024-01297-9

[3] Shokrani, A., Dogan, H., Burian, D., Nwabueze, T. D., Kolar, P., Liao, Z., Sadek, A., Teti, R., Wang, P., Pavel, R., & Schmitz, T. (2024). Sensors for in-process and on-machine monitoring of machining operations. CIRP Journal of Manufacturing Science and Technology, 51, 263-292. https://doi.org/10.1016/j.cirpj.2024.05.001

[4] Liu, Z., Lang, Z.-Q., Gui, Y., Zhu, Y.-P., & Laalej, H. (2024). Digital twin-based anomaly detection for real-time tool condition monitoring in machining. Journal of Manufacturing Systems, 75, 163-173. https://doi.org/10.1016/j.jmsy.2024.06.004

[5] Surindra, M. D., Alfarisy, G. A. F., Caesarendra, W., Petra, M. I., Prasetyo, T., Tjahjowidodo, T., Królczyk, G. M., Glowacz, A., & Gupta, M. K. (2025). Use of machine learning models in condition monitoring of abrasive belt in robotic arm grinding process. Journal of Intelligent Manufacturing, 36(5), 3345-3358. https://doi.org/10.1007/s10845-024-02410-6

[6] Kannan, V., Dao, D. V., & Li, H. (2024). Detection of Signal Integrity Issues in Vibration Monitoring Using One-Class Support Vector Machine. Journal of Vibration Engineering & Technologies, 12(S1), 601-611. https://doi.org/10.1007/s42417-024-01435-8

[7] Waszak, M., Moen, T., Hansen, A. H., Bouquet, G., Pultier, A., Ma, X., & Roman, D. (2024). Vibration Sensors for Detecting Critical Events: A Case Study in Ferrosilicon Production. IEEE Access, 12, 12465-12477. https://doi.org/10.1109/access.2024.3356067

[8] Oikonomou, D., Leontaris, L., Dimitriou, N., & Tzovaras, D. (2025). Time-Series Forecasting in Industrial Environments: A Performance Study and a Novel Late Fusion Framework. IEEE Sensors Journal, 25(4), 7681-7697. https://doi.org/10.1109/jsen.2025.3526362

[9] Jiang, Z., Ning, Z., Miao, H., & Wang, L. (2024). STDNet: A Spatio-Temporal Decomposition Neural Network for Multivariate Time Series Forecasting. Tsinghua Science and Technology, 29(4), 1232-1247. https://doi.org/10.26599/tst.2023.9010105

[10] Yan, H., Zhou, H., Zheng, J., & Zhou, Z. (2025). Rolling Bearing Fault Diagnosis Based on 1D Convolutional Neural Network and Kolmogorov–Arnold Network for Industrial Internet. Computers, Materials & Continua, 83(3), 4659-4677. https://doi.org/10.32604/cmc.2025.062807

[11] Soprani, D., Santos, K., Macedo, L., Villani, L. G. G., Leal-Junior, A., & Frizera-Neto, A. (2026). Comparing Fiber Bragg Grating and Piezoelectric Vibration Sensors Using Multilayer Perceptron and Kolmogorov–Arnold Network Models for Rotating Machinery Fault Diagnosis. Journal of Lightwave Technology, 44(7), 2790-2802. https://doi.org/10.1109/jlt.2025.3634028

[12] Mansouri, M., Attouri, K., & Kouadri, A. (2026). Efficient Fault Diagnosis in Industrial Systems Using Enhanced PolyKAN Techniques. IEEE Transactions on Industrial Informatics, 22(3), 2311-2322. https://doi.org/10.1109/tii.2025.3639486

[13] Collao, C., Akhtar, H., Toro, C., Ocampo-Martínez, C., Schor, R., & Prieto, R. P. (2025). An Agentic AI-based Architecture for Digital Twins Specialized in Predictive Maintenance: Application to Ball Mills. IFAC-PapersOnLine, 59(32), 96-101. https://doi.org/10.1016/j.ifacol.2025.12.403

[14] Le, V., Tran, M., & Ding, S. (2024). Subtractive manufacturing of composite materials with robotic manipulators: a comprehensive review. The International Journal of Advanced Manufacturing Technology, 135(1-2), 81-117. https://doi.org/10.1007/s00170-024-14427-5

[15] Krajnik, P., Wegener, K., Bergs, T., & Shih, A. J. (2024). Advances in modeling of fixed-abrasive processes. CIRP Annals, 73(2), 589-614. https://doi.org/10.1016/j.cirp.2024.05.001

[16] Shao, Z., Wang, F., Xu, Y., Wei, W., Yu, C., Zhang, Z., Yao, D., Sun, T., Jin, G., Cao, X., Cong, G., Jensen, C. S., & Cheng, X. (2025). Exploring Progress in Multivariate Time Series Forecasting: Comprehensive Benchmarking and Heterogeneity Analysis. IEEE Transactions on Knowledge and Data Engineering, 37(1), 291-305. https://doi.org/10.1109/tkde.2024.3484454

[17] Leite Coelho da Silva, F., da Silva Cordeiro, J., da Costa, K., Saboya, N., Canas Rodrigues, P., & López-Gonzales, J. L. (2025). Time series forecasting via integrating a filtering method: an application to electricity consumption. Computational Statistics, 40(9), 5023-5042. https://doi.org/10.1007/s00180-024-01595-x

[18] Wang, X., Hyndman, R. J., & Wickramasuriya, S. L. (2025). Optimal forecast reconciliation with time series selection. European Journal of Operational Research, 323(2), 455-470. https://doi.org/10.1016/j.ejor.2024.12.004

[19] Yun, H., Giurcăneanu, C. D., & Dobbie, G. (2025). Novel indicators for monitoring bearing condition using frequency-domain dictionary learning. The International Journal of Advanced Manufacturing Technology, 140(7-8), 3941-3963. https://doi.org/10.1007/s00170-025-16534-3

[20] Luan, X., Zhao, J., Sha, Y., & Liu, M. (2026). Rolling bearing state monitoring method based on fusion of multichannel vibration signals with oil debris information. Structural Health Monitoring, 25(3), 2129-2152. https://doi.org/10.1177/14759217241301305

[21] Huang, R., Ma, L., Hu, J., Duan, X., Gao, H., & Ma, J. (2025). Diagnosis of unbalanced bearing fault samples based on cycle generative adversarial networks. Neural Computing and Applications, 37(19), 13447-13467. https://doi.org/10.1007/s00521-025-11265-8

[22] Fang, K., Tong, L., Xu, X., Cai, J., Peng, X., Omar, M., Kashif Bashir, A., & Wang, W. (2025). Robust Fault Diagnosis of Drilling Machinery Under Complex Working Conditions Based on Carbon-Intelligent Industrial Internet of Things. IEEE Internet of Things Journal, 12(17), 34663-34678. https://doi.org/10.1109/jiot.2025.3542404

[23] Li, X., Chen, J., Wang, J., Wang, J., Li, X., & Kan, Y. (2024). Research on Fault Diagnosis Method of Bearings in the Spindle System for CNC Machine Tools Based on DRSN-Transformer. IEEE Access, 12, 74586-74595. https://doi.org/10.1109/access.2024.3404968

[24] Kisten, M., Ezugwu, A. E.-S., & Olusanya, M. O. (2024). Explainable Artificial Intelligence Model for Predictive Maintenance in Smart Agricultural Facilities. IEEE Access, 12, 24348-24367. https://doi.org/10.1109/access.2024.3365586

[25] Yan, P., Abdulkadir, A., Luley, P.-P., Rosenthal, M., Schatte, G. A., Grewe, B. F., & Stadelmann, T. (2024). A Comprehensive Survey of Deep Transfer Learning for Anomaly Detection in Industrial Time Series: Methods, Applications, and Directions. IEEE Access, 12, 3768-3789. https://doi.org/10.1109/access.2023.3349132

[26] Marahatta, S., Albagdady, A., Zheng, D., & Liu, H. (2026). Tracking Recovery: An Up-to-Date Overview of Wearable Sensors in Healthcare Monitoring for Post-Stroke Patients—A Review. IEEE Sensors Journal, 26(2), 1449-1464. https://doi.org/10.1109/jsen.2025.3634992

[27] Papananias, M. (2025). Bayesian monitoring of machining processes using non-intrusive sensing and on-machine comparator measurement. The International Journal of Advanced Manufacturing Technology, 137(3-4), 1929-1942. https://doi.org/10.1007/s00170-025-15174-x